



# Visualization of Temperature and Flow Behavior in a Continuous Pasteurizer Using Computation Fluid Dynamics

Emmanuel Baidhe, Julia Kigozi, Hussein Kivumbi Balimunsi

Department of Agricultural and Biosystems Engineering, Makerere University Kampala, Kampala, Uganda  
Email: emmanuel.baidhe@students.mak.ac.ug

**How to cite this paper:** Baidhe, E., Kigozi, J. and Balimunsi, H.K. (2022) Visualization of Temperature and Flow Behavior in a Continuous Pasteurizer Using Computation Fluid Dynamics. *Open Access Library Journal*, 9: e8888.  
<https://doi.org/10.4236/oalib.1108888>

**Received:** May 16, 2022

**Accepted:** September 18, 2022

**Published:** September 21, 2022

Copyright © 2022 by author(s) and Open Access Library Inc.

This work is licensed under the Creative Commons Attribution International License (CC BY 4.0).

<http://creativecommons.org/licenses/by/4.0/>



Open Access

## Abstract

The holding tube and heat exchangers are the most significant components in High-Temperature-Short-Time (HTST) pasteurization processes as they ensure that the system adheres to the set temperature and time conditions. The purpose of this study was to visualize the temperature and flow behavior in heat exchangers and the holding tube of the continuous pasteurizer. The pasteurizer consists of three heat exchangers (heating, regeneration, and cooling section) operating on a counter-current flow system. SolidWorks 2019 was used for both modeling and simulation. There was a significant increase ( $p < 0.05$ ) in tube-side fluid temperature in the heating and regeneration section. A significant reduction ( $p < 0.05$ ) in tube-side fluid temperature was also observed in the cooling section. There was no significant variation ( $p < 0.05$ ) in tube-side and shell-side velocities along with the different passes for all heat exchangers. A significant pressure drop ( $p < 0.05$ ) was observed with the tube-side and shell-side fluids for all heat exchangers. Simulation of flow in the holding tube revealed that the fluid had relatively uniform velocity (0.086 - 0.129 m/s) and temperature of 87.9°C, but with a reduction in fluid pressure. There are high-pressure drops at the U-bends than along the straight path in the holding tubes. The current design has the potential to facilitate heat transfer and maintain the predetermined holding temperature.

## Subject Areas

Engineering and Simulation

## Keywords

High-Temperature-Short-Time, Pasteurization, Holding Tube and Heat Exchangers, Simulation

## 1. Introduction

Pasteurization is considered a critical unit operation in the juice processing chain as it extends the shelf life of the juice. Pasteurization involves reducing the number of viable pathogens in a food product by using relatively low temperatures [1]. Pasteurization as opposed to sterilization aims to kill pathogenic microbes and reduce the number of spoilage organisms in the food while maintaining food quality [2] [3]. Heat exchangers facilitate heat transfer during pasteurization, thus regulating fluid temperatures within the systems [4].

Pasteurization, the world over is done by either the batch or continuous pasteurizer. Continuous pasteurizers are becoming more popular than batch pasteurizers due to their continuous throughput, which enhances operational efficiency by reducing actual processing time and labor needs [5] [6]. Continuous pasteurization is the process of passing food through a series of heat exchange systems. It is designed to handle a large volume of food product, making it more suitable for industrial production. Continuous pasteurization has several advantages over batch pasteurization, including 1) the ability to reduce production time and energy requirement, 2) the ability to package product as soon as pasteurization is complete, 3) ease of cleaning and sanitizing using clean-in-place (CIP), 4) low operational costs due to the regeneration system, and 5) reduced product losses [7]. Continuous pasteurization is a High-Temperature-Short-Time (HTST) process, thus bacteria in the product are killed with minimal impact on the flavor and nutrient concentration [1] [6].

Notwithstanding the benefits of using continuous pasteurization, its adoption in Uganda is still constrained by the limited access to the appropriate equipment. All continuous pasteurizers have to be imported from Europe and Asia (China). This, however, comes at a hefty cost of importing, such as taxes. Furthermore, because this is not native technology, maintenance is difficult as the equipment can only be serviced by specialist experts, who must be outsourced. This warrants the development of local continuous pasteurization technology that responds to the needs of local consumers in Uganda.

Previous pasteurization research in Uganda concentrated on the development of batch pasteurizers [8] [9]. Though efficient for production, the batch system is associated with a lot of drudgery (labor, time, and energy) [1]. During the process of cooling the product prior to packaging, a lot of waste heat is generated [10]. To enable the small-scale processors in Uganda to tap into the benefits of continuous pasteurization, the Department of Agricultural and Biosystems Engineering, Makerere University embarked on the design and development of a small-scale low-viscous juice continuous pasteurizer. Since continuous pasteurization is so dependent on temperature and flow (velocity and pressure), these parameters must be taken into account during the design process. However, analysis of fluid motion is sometimes complex [11]. Modeling and simulation using could be incredibly beneficial tools for exploiting temperature and flow behavior [12] [13], two critical factors that determine the output of a continuous

pasteurization system. It is, therefore, easier to attempt to establish its behavior using flow simulation software. The simulation works on a mathematical model that describes the system. The use of software for flow simulation is collectively referred to as Computational Fluid Dynamics (CFD). Computational Fluid Dynamics is widely used to determine the temperature and flow profiles by identifying the locations with the least amount of heat distribution [14] [15]. CFD uses the Navier-Stokes equation (Equation (1)). These equations are used to solve the equations for conservation of mass, momentum and energy for the required system [16]. Therefore, the purpose of this study was to visualize the temperature, velocity, and pressure distribution in heat exchangers as well as the holding tube of the continuous pasteurizer.

$$\left(\frac{\partial \rho \phi}{\partial t}\right) + \left(\frac{\partial \rho u \phi}{\partial x} + \frac{\partial \rho v \phi}{\partial y} + \frac{\partial \rho w \phi}{\partial z}\right) = \Gamma \left(\frac{\partial^2 \phi}{\partial x^2} + \frac{\partial^2 \phi}{\partial y^2} + \frac{\partial^2 \phi}{\partial z^2}\right) + S(\phi) \quad (1)$$

where,  $\phi = 1$ ,  $V(u, v, w)$ ,  $\Gamma$  for mass, momentum and energy equations respectively.

## 2. Description and Mode of Operation of the Continuous Pasteurizer

### 2.1. Description of the Continuous Pasteurizer

The continuous pasteurizer consists of three heat exchangers (heating, regeneration, and cooling sections), two tanks (juice and hot water tank), a hot water tank, a control panel, two pumps (Hot water pump and juice pump), a holding tube, heaters, reservoir, and several piping to allow material flow on both the hot and cold sides [4]. These parts are all attached to the mainframe. The heat exchangers are of shell and tube type running under counter-flow to enhance heat transfer within the pasteurizer [17]. The shells and tubes are of square and elliptical cross-sections, respectively. The characteristic features for each of the sections are shown in **Table 1**. The regenerating section was added to recover waste heat that could otherwise be lost during the cooling process [10]. The pasteurizer is coupled with a holding tube where the juice runs at relatively low speeds to allow time for the destruction of micro-organisms [18].

### 2.2. Mode of Operation for the Continuous Pasteurizer

The method of operation was inspired by the existing continuous pasteurizer at Makerere University's Food Technology and Business Incubation Center (FTBIC). A more user-friendly and tailored mode of operation was developed using incremental innovative design principles, as discussed in this section. Incremental innovation is a low-risk adoption process, therefore less likely to fail over time [19].

The heating medium (water) is heated for a set duration before being pumped through the heating section, allowing heat to be delivered to the juice during pasteurization. A juice pump transfers raw juice from the juice tank to the rege-

neration section, where it is preheated with hot juice. The juice next passes through the heating section, where it is heated to a pasteurization temperature set by the user. The juice is then held at the same temperature for a short time in the holding tubes before being cooled in the regeneration and cooling section (Figure 1).

### 3. Material and Methods

#### 3.1. Modeling and Simulation of the Pasteurization Process

SolidWorks 2019 was used for both modeling and simulation, as it is simple and robust, allowing the user to perform all steps such as creating parts, assemblies, and simulations [11] [20]. The different components of the pasteurizer were

**Table 1.** Summary of the heat exchanger characteristics.

Heat exchanger section	Heating	Regeneration	Cooling
No. of shells	4	3	2
No. of tubes	16	12	8
No. of shell passes	4	3	2
No. of tube passes	8	6	4
No. of tube per pass	2	2	2

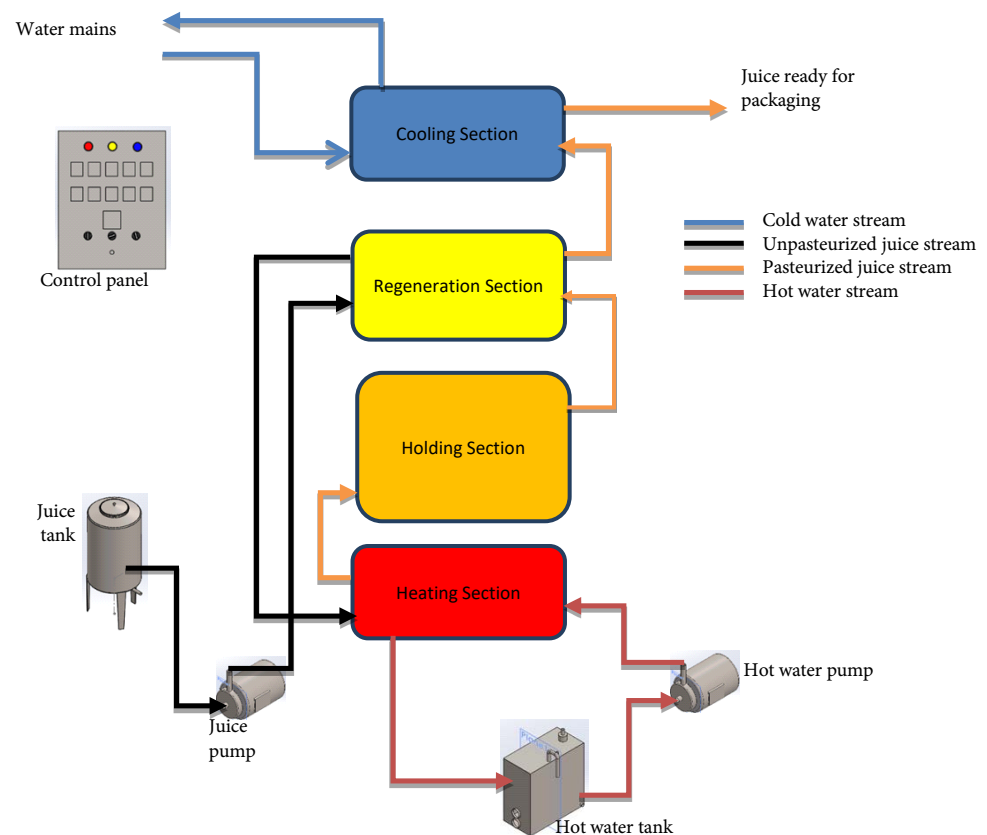


**Figure 1.** Schematic illustration of the mode of operation of the continuous pasteurizer.

modeled in SolidWorks Part and assembled in SolidWorks Assembly. SolidWorks Drawing was used to create the design drawing for the equipment's production. The simulation was done for the three heat exchangers and the holding tube. Heat exchangers enable the actual heat transfer from the hot to the cold medium during pasteurization. The holding tube provides a defined length of piping to "retain" a product at a specific flow rate, at not less than the pasteurizing temperature, for a predetermined amount of time [18]. Therefore, both heat exchangers and the holding tube are the most important components for HTST pasteurization processes as they ensure adherence of the system to the set temperature and time conditions.

Simulation of heat transfer and flow was done using Flow simulation add-in tool embedded into the SolidWorks 2019 following the procedure below as described in Matsson [21]; 1) SolidWorks flow simulation was selected from Tools tab, 2) The model was sealed off using lids and checked for tightness using the check geometry tool, 3) A new flow simulation project was created using the Wizard tool. This involved setting the project configuration, the unit system to International System (SI) Units, analysis type to Internal. The default fluid used was water. The default wall conditions such as thermal condition (adiabatic) and roughness (0  $\mu\text{m}$ ) were maintained. The initial conditions for flow parameters were maintained in the default (Pressure and temperature at 101.335 kPa and 293.2 K (20.2°C), respectively). At this point, the project was set for simulation, 4) Using the SolidWorks flow simulation design tree tab, the boundary conditions such as mass flow rate were set for the inlet as shown in Table 2 and environmental pressure at outlet points set at 101.325 kPa. The surface goals for temperature, velocity, and pressure at a minimum, average and maximum, 5) The flow was run to solve the calculation, 6) After the calculation was completed, the results were loaded for preview. Flow trajectories and contours cut plots were inserted for temperature, velocity, and pressure.

**Table 2.** Boundary conditions for the inlet of the different pasteurizer components.

Boundary condition	Pasteurizer components						
	Heating section		Regeneration section		Cooling section		Holding tube
	Tube-side	Shell-side	Tube-side	Shell-side	Tube-side	Shell-side	
Mass flow rate (kg/s)	0.1 <sup>e</sup>	0.34 <sup>f</sup>	0.14 <sup>f</sup>	0.1 <sup>g</sup>	0.1 <sup>e</sup>	0.16 <sup>f</sup>	0.1 <sup>g</sup>
Temperature (°C)	50 <sup>b</sup>	100 <sup>c</sup>	27 <sup>a</sup>	88 <sup>d</sup>	55 <sup>b</sup>	27 <sup>a</sup>	88 <sup>d</sup>

<sup>a</sup> Ambient temperature based on Uganda; <sup>b</sup> Estimated based on preliminary testing of an existing imported continuous pasteurizer; <sup>c</sup> Boiling point for water; <sup>d</sup> Pasteurization temperature for juice under HTST [1] [22]; <sup>e</sup> Estimated based on the threshold value for laminar flow ( $Re < 2100$ ); <sup>f</sup> Based on design calculations; <sup>g</sup> Based on the exit flow rate of juice from the heating section.

### 3.2. Data Collection and Analysis

The tubes and shells passes were named based on the flows. The first and last pass occurred at the entry and exit of the tube flow respectively. The first and last shells are those where the shell fluid enters and leaves the heat exchanger section respectively. The same procedure was applied for heating, regeneration and cooling section (Figure 2).

Using the probe, the tube and shell-side fluid temperature in the heating section heat exchanger was determined from the temperature cut plot at 6 different points (T1 to T6) along the length of each tube and shell using the probe (Figure 2). The process was repeated for velocity and pressure profiles using the velocity and pressure cut plots, respectively. The above procedure was repeated for the regeneration, and cooling section heat exchangers. The data collected was checked for normality by plotting the residual plots. The produced residual plots were normally distributed about the mean with variances being homogeneous, which meets the assumptions of analysis of variance (ANOVA). Analysis of variance (ANOVA) was used to determine the significant difference in temperature, velocity, and pressure for different tube and shell passes ( $p < 0.05$ ).

## 4. Results and Discussion

### 4.1. Simulation of Temperature and Flow in the Heating Section

#### 4.1.1. Tube-Side Fluid Temperature, Velocity, and Pressure for the Heating Section

The results of the temperature, velocity, and pressure simulation for the heating

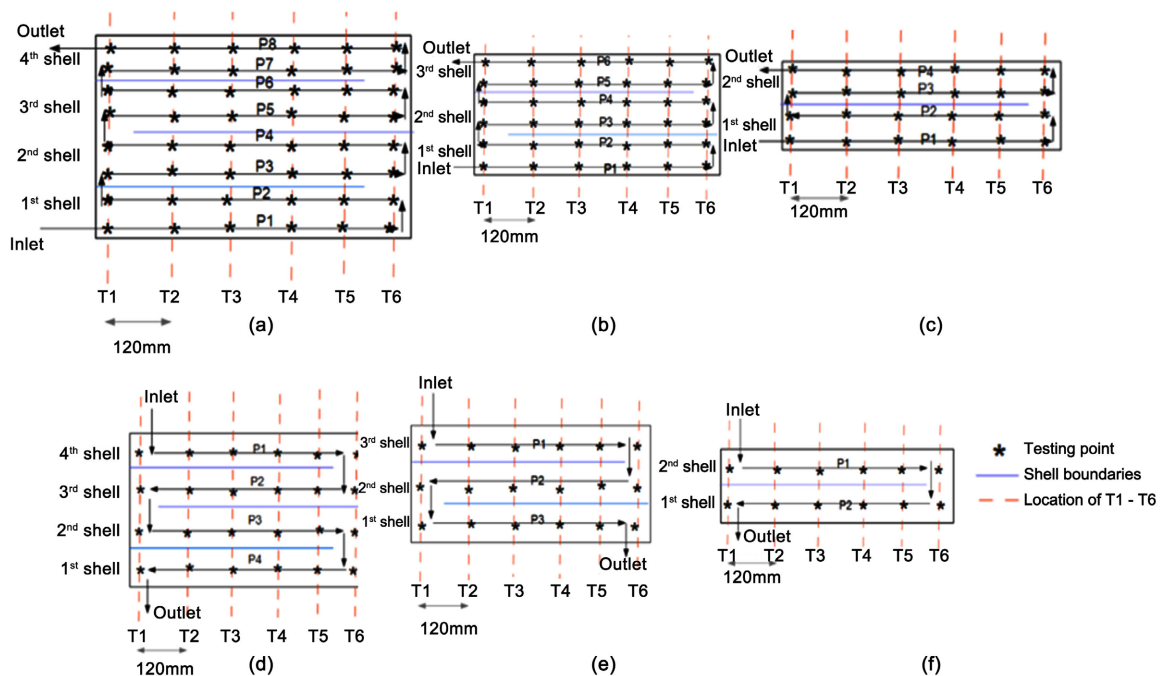
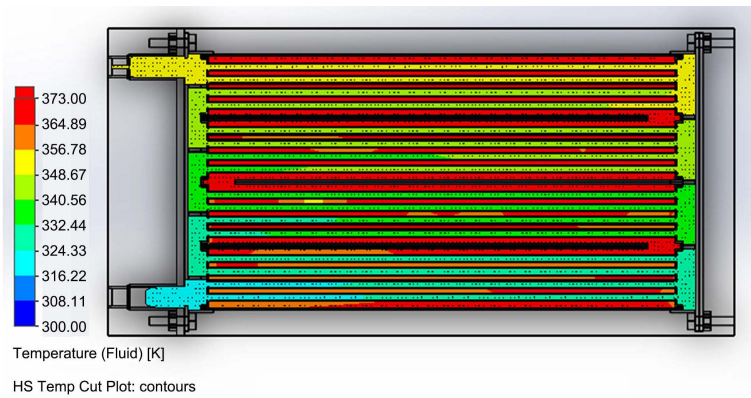
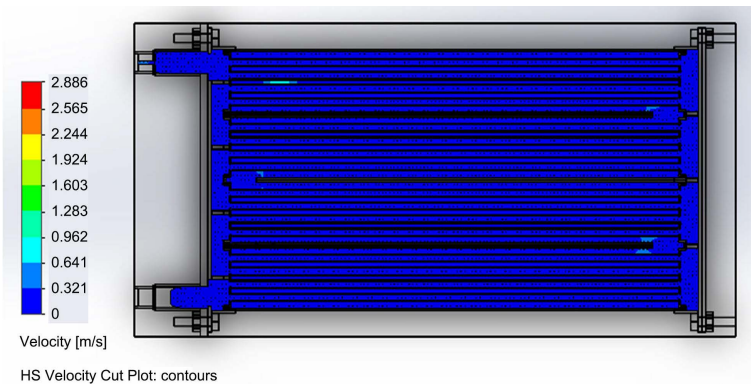


**Figure 2.** Illustration of the testing locations, testing points, and passes (a) Tube passes under heating section, (b) Tube passes under regeneration section, (c) Tube passes under cooling section, (d) Shell passes in heating section, (e) Shell passes in the regeneration system, (f) Shell passes in the cooling system.

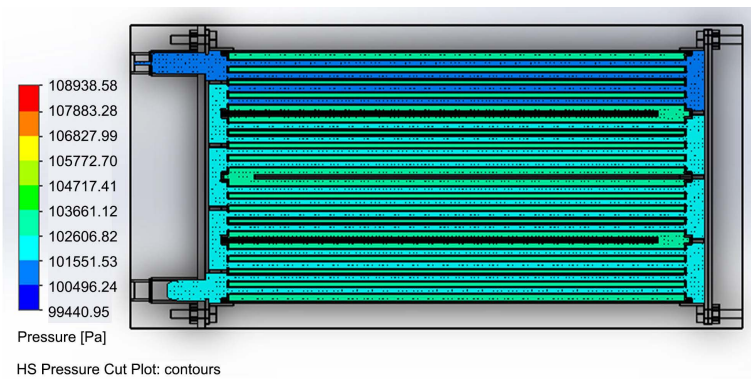
section are shown by the contour cut plots in **Figure 3**. The preheated tube-side fluid entered and exited the heat exchanger at temperatures of 50.29°C and 81.75°C, respectively. The fluid temperature increased along the pass for all eight passes (**Figure 3(a)**). The fluid temperature increased significantly ( $p < 0.05$ ) from the first to the eighth pass (**Table 3**). The mean fluid temperature was found to be 51.98°C, 56.48°C, 60.77°C, 64.46°C, 68.30°C, 71.56°C, 74.65°C, 78.7°C along with the first, second, third, fourth, fifth, sixth, seventh, and eighth pass, respectively.



(a)



(b)



(c)

**Figure 3.** Contour cut plots for the heating section heat exchanger (a) Temperature, (b) Velocity, (c) Pressure.

**Table 3.** Variation of tube-side and shell-side temperature, velocity, and pressure along the fluid passes within the heating section.

Pass	Tube-side (Mean $\pm$ SD)			Shell-side (Mean $\pm$ SD)		
	Temperature ( $^{\circ}$ C)	Velocity (m/s)	Pressure (kPa)	Temperature ( $^{\circ}$ C)	Velocity (m/s)	Pressure (kPa)
P1	51.98 $\pm$ 1.430 <sup>a</sup>	0.137 $\pm$ 0.0668 <sup>a</sup>	101.9 $\pm$ 0.0216 <sup>h</sup>	95.45 $\pm$ 0.456 <sup>a</sup>	0.0493 $\pm$ 0.0380 <sup>a</sup>	103.6 $\pm$ 0.0046 <sup>d</sup>
P2	56.48 $\pm$ 1.418 <sup>b</sup>	0.150 $\pm$ 0.0665 <sup>a</sup>	101.9 $\pm$ 0.0276 <sup>g</sup>	92.28 $\pm$ 0.452 <sup>b</sup>	0.0495 $\pm$ 0.0411 <sup>a</sup>	103.5 $\pm$ 0.0025 <sup>c</sup>
P3	60.77 $\pm$ 1.638 <sup>c</sup>	0.158 $\pm$ 0.0702 <sup>a</sup>	101.8 $\pm$ 0.0237 <sup>f</sup>	93.13 $\pm$ 0.964 <sup>b</sup>	0.0605 $\pm$ 0.0366 <sup>a</sup>	103.4 $\pm$ 0.0039 <sup>b</sup>
P4	64.46 $\pm$ 1.311 <sup>d</sup>	0.151 $\pm$ 0.0640 <sup>a</sup>	101.7 $\pm$ 0.0200 <sup>e</sup>	87.91 $\pm$ 1.306 <sup>c</sup>	0.0483 $\pm$ 0.0184 <sup>a</sup>	103.3 $\pm$ 0.0042 <sup>a</sup>
P5	68.30 $\pm$ 1.371 <sup>e</sup>	0.146 $\pm$ 0.0719 <sup>a</sup>	101.7 $\pm$ 0.0204 <sup>d</sup>			
P6	71.56 $\pm$ 1.142 <sup>f</sup>	0.134 $\pm$ 0.0587 <sup>a</sup>	101.6 $\pm$ 0.0262 <sup>c</sup>			
P7	74.65 $\pm$ 1.160 <sup>g</sup>	0.140 $\pm$ 0.140 <sup>a</sup>	101.5 $\pm$ 0.0255 <sup>b</sup>			
P8	78.7 $\pm$ 2.241 <sup>h</sup>	0.157 $\pm$ 0.0675 <sup>a</sup>	101.5 $\pm$ 0.0257 <sup>a</sup>			
p-value	<0.001	0.997	<0.001	<0.001	0.919	<0.001

P1, P2, P3, P4, P5, P6, P7, and P8 are the first, second, third, fourth, fifth, sixth, seventh, and eighth pass respectively. Means in the same column with different superscripts are significantly different ( $p < 0.05$ ).

The mean tube-side velocities were higher compared to those of the shell-side (Table 3). The tube-side fluid entered the heat exchanger at 0.051 m/s and exited at 0.085 m/s. The velocity at the turning points was observed to be low compared to that within the tubes (Figure 3(b)). Within the tubes, the mean tube-side velocity did not differ significantly ( $p < 0.05$ ) from one tube pass to another (Table 3). The mean tube-side velocity was maintained at 0.137 m/s, 0.15 m/s, 0.158 m/s, 0.151 m/s, 0.146 m/s, 0.134 m/s, 0.14 m/s, 0.157 m/s along the first, second, third, fourth, fifth, sixth, seventh, and eighth passes, respectively.

The tube-side fluid entered and exited the heating section at 101.96 kPa and 101.433 kPa, respectively. For all the eight passes, the tube-side fluid pressure was initially high at the start of the pass, but dropped steadily and remained nearly constant throughout the pass (Figure 3(c)). A significant pressure drop ( $p < 0.05$ ) was observed from the first to eighth tube pass (Table 3). The mean pressure 101.9 kPa, 101.9 kPa, 101.8 kPa, 101.7 kPa, 101.6 kPa, 101.5 kPa, 101.5 kPa, for the first, second, third, fourth, fifth, sixth, seventh, and eighth pass, respectively.

#### 4.1.2. Shell-Side Fluid Temperature, Velocity, and Pressure for the Heating Section

The shell-side fluid was at a higher temperature than the tube-side fluid (Table 3). The shell-side fluid temperature was relatively dropped as the fluid crossed from the first to the second pass. A similar observation was made as the fluid crossed from third to fourth pass (Figure 3(a)). The mean fluid temperature was found to be 95.45 $^{\circ}$ C, 92.28 $^{\circ}$ C, 93.13 $^{\circ}$ C, and 87.97 $^{\circ}$ C along with the first, second, third, and fourth pass, respectively. The shell-side fluid temperature reduced significantly ( $p < 0.05$ ) from the first to the fourth pass shell pass of the heating section (Table 3). Post-hoc analysis indicated that the shell-side temperature in

the first pass was significantly higher ( $p < 0.05$ ) compared to that of the second, third, and fourth pass. However, the shell-side temperatures for the second and the third pass were not significantly different ( $p < 0.05$ ) (**Table 3**).

It was observed that the shell-side velocity varied continuously within the range of 0.01 m/s and 0.13 m/s for all the passes (**Figure 3(b)**). The mean shell-side velocity increased towards the second and third pass but eventually dropped on the final pass. However, there was no significant variation ( $p < 0.05$ ) in shell-side velocity for the four shell passes in the heating section (**Table 3**). The mean shell-side velocity was found to be 0.0493 m/s, 0.0495 m/s, 0.605 m/s, 0.0483 m/s along the first, second, third, and fourth pass, respectively.

The shell-side fluid pressure is observed to be relatively uniform within the tubes, but with drastic drops at the first-second, second-third, and third-fourth turning points (**Figure 3(c)**). The mean shell-side fluid pressure in the first, second, third, and fourth pass was 103.6 kPa, 103.5 kPa, 103.4 kPa, and 103.3 kPa, respectively. A significant pressure drop ( $p < 0.05$ ) was observed from the first to the fourth shell pass (**Table 3**).

## 4.2. Simulation of Temperature and Flow in the Regeneration Section

### 4.2.1. Tube-Side Fluid Temperature, Velocity, and Pressure for the Regeneration Section

**Figure 4** shows the contour cut plots for the temperature, velocity, and pressure profiles for the regeneration section heat exchanger. From **Figure 4(a)**, the tube-side fluid temperature increased gradually along the tubes, as is the case from one pass to another. The tube-side fluid temperature increased significantly ( $p < 0.05$ ) by tube pass (**Table 4**). The mean temperature was 28.21°C, 30.44°C, 33.08°C, 35.63°C, 38.62°C, and 41.17°C for the first, second, third, fourth, fifth, and sixth tube pass, respectively.

The tube-side velocity was high within the tubes compared to entry and exit points (**Figure 4(b)**). The mean tube-side velocity was found to be 0.235 m/s, 0.220 m/s, 0.212 m/s, 0.230 m/s, 0.210 m/s, and 0.232 m/s along the first, second, third, fourth, fifth, and sixth pass respectively. However, there was no significant difference ( $p < 0.05$ ) in velocities for the different passes (**Table 4**).

The tube-side fluid experienced a gradual pressure drop along the tubes, for all passes (**Figure 4(c)**), though with significant pressure drop ( $p < 0.05$ ) from one pass to another (**Table 4**). The mean pressure was found to be 102.2 kPa, 102.1 kPa, 101.9 kPa, 101.8 kPa, 101.6 kPa, and 101.5 kPa for the first, second, third, fourth, fifth, and sixth pass, respectively.

### 4.2.2. Shell-Side Fluid Temperature, Velocity, and Pressure for the Regeneration Section

From **Figure 4(a)**, the temperature for the shell-side fluid was observed to reduce along with the passes. The mean temperature was observed to be at 77.22°C, 68.23°C, and 60.77°C for the first, second, and third pass, respectively.

A significant reduction ( $p < 0.05$ ) in the shell-side fluid temperature is observed from the first to the third shell pass. The temperatures at the first and third passes were significantly different ( $p < 0.05$ ). The temperature at the second pass, however, did not differ significantly ( $p < 0.05$ ) from that of the first and third pass (**Table 4**).

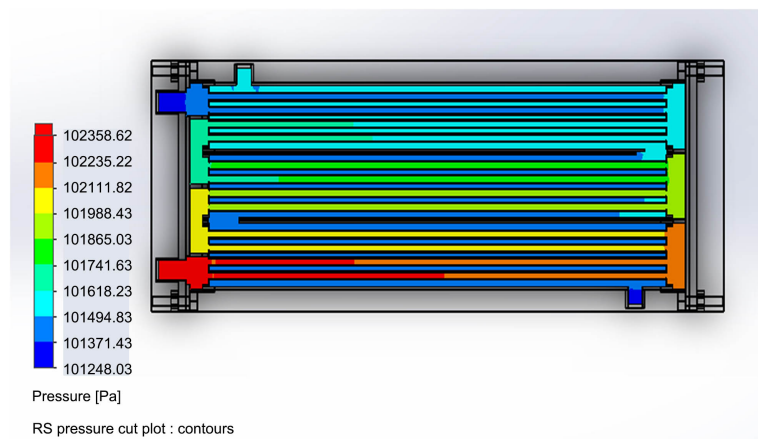
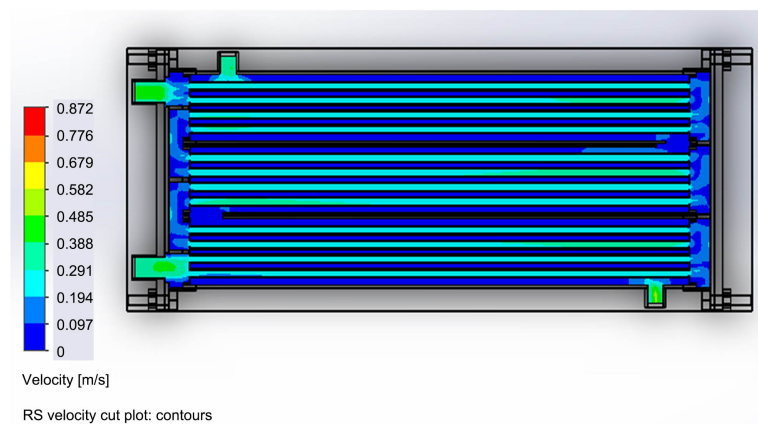
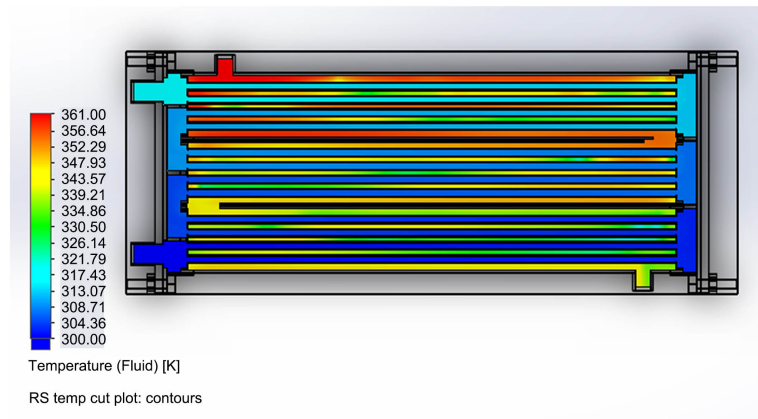


**Figure 4.** Contour cut plots for the regeneration section heat exchanger (a) Temperature, (b) Velocity, (c) Pressure.

The shell-side velocity was observed to drop steadily from the first to the third pass (Figure 4(b)). The mean shell-side velocity was found to be 0.0215 m/s, 0.018 m/s, and 0.015 m/s along with the first, second, and third pass, respectively. From Table 4, there was no significant variation ( $p < 0.05$ ) in shell-side velocity for the three passes in the regeneration section.

The shell-side fluid maintained a steady pressure within the tubes for the first, second, and third pass. There was a pressure drop as the fluid crossed from one shell passed to another (Figure 4(c)). The mean shell-side fluid pressure in the first, second, and third shell pass was 101.506 kPa, 101.493 kPa, and 101.484 kPa, respectively. There was a significant reduction in the pressures ( $p < 0.05$ ) from the first to the third pass (Table 4).

### 4.3. Simulation of Temperature and Flow in the Cooling Section

#### 4.3.1. Tube-Side Fluid Temperature, Velocity, and Pressure in the Cooling Section

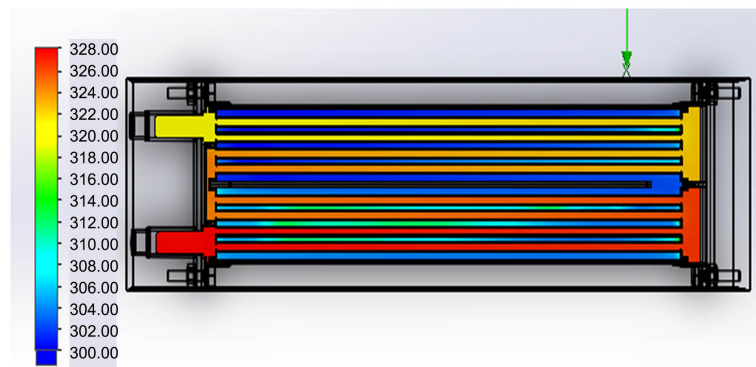
Figure 5 shows the contour cut plots for the temperature, velocity, and pressure for the cooling section heat exchanger. The temperature of the tube-side fluid was higher than the shell-side fluid temperature (Table 5). There was a gradual reduction in temperature along the tube pass, for all tube-side passes (Figure 5(a)). The mean temperatures in the 54.23 °C, 52.06 °C, 50.11 °C, and 48.25 °C for the first, second, third, and fourth pass, respectively. Analysis of variance indicated that temperature varied significantly ( $p < 0.05$ ) with tube passes (Table 5).

The tube-side fluid velocity was higher along the pass than the start and end of the pass. A similar trend was observed for all the four-tube passes (Figure 5(b)). The velocity at the turning points was observed to be low compared to that within the tubes (Figure 5(b)). The mean tube-side velocity was maintained at 0.161 m/s, 0.149 m/s, 0.154 m/s, and 0.137 m/s along with the first, second, third, and fourth passes, respectively. However, there was no significant difference ( $p < 0.05$ ) in the fluid velocities for all four passes (Table 5).

**Table 4.** Variation of tube-side and shell-side temperature, velocity, and pressure along the fluid passes within the regeneration section.

Pass	Tube-side (Mean $\pm$ SD)			Shell-side (Mean $\pm$ SD)		
	Temperature (°C)	Velocity (m/s)	Pressure (kPa)	Temperature (°C)	Velocity (m/s)	Pressure (kPa)
P1	28.21 $\pm$ 0.825 <sup>a</sup>	0.235 $\pm$ 0.0766 <sup>a</sup>	102.2 $\pm$ 0.0379 <sup>f</sup>	77.22 $\pm$ 5.617 <sup>b</sup>	0.0215 $\pm$ 0.0108 <sup>a</sup>	101.5 $\pm$ 0.0001 <sup>c</sup>
P2	30.44 $\pm$ 0.721 <sup>b</sup>	0.220 $\pm$ 0.107 <sup>a</sup>	102.1 $\pm$ 0.0492 <sup>e</sup>	68.23 $\pm$ 5.516 <sup>ab</sup>	0.018 $\pm$ 0.0091 <sup>a</sup>	101.5 $\pm$ 0.0004 <sup>b</sup>
P3	33.08 $\pm$ 0.813 <sup>c</sup>	0.212 $\pm$ 0.108 <sup>a</sup>	101.9 $\pm$ 0.0475 <sup>d</sup>	60.77 $\pm$ 7.521 <sup>a</sup>	0.015 $\pm$ 0.0091 <sup>a</sup>	101.5 $\pm$ 0.0007 <sup>a</sup>
P4	35.63 $\pm$ 0.901 <sup>d</sup>	0.230 $\pm$ 0.0879 <sup>a</sup>	101.8 $\pm$ 0.0536 <sup>c</sup>			
P5	38.62 $\pm$ 0.951 <sup>e</sup>	0.21 $\pm$ 0.0868 <sup>a</sup>	101.6 $\pm$ 0.0445 <sup>b</sup>			
P6	41.17 $\pm$ 1.004 <sup>f</sup>	0.232 $\pm$ 0.0812 <sup>a</sup>	101.5 $\pm$ 0.0486 <sup>a</sup>			
p-value	< 0.001	0.995	< 0.001	0.002	0.509	< 0.001

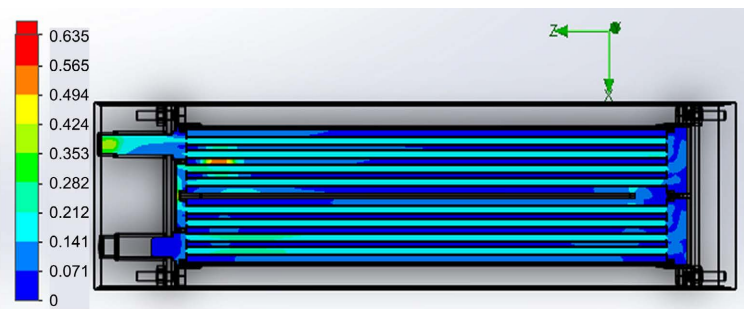
P1, P2, P3, P4, P5, and P6 are the first, second, third, fourth, fifth, and sixth pass respectively. Means in the same column with different superscripts are significantly different ( $p < 0.05$ ).



Temperature (Fluid) [K]

CS temp cut plot: contours

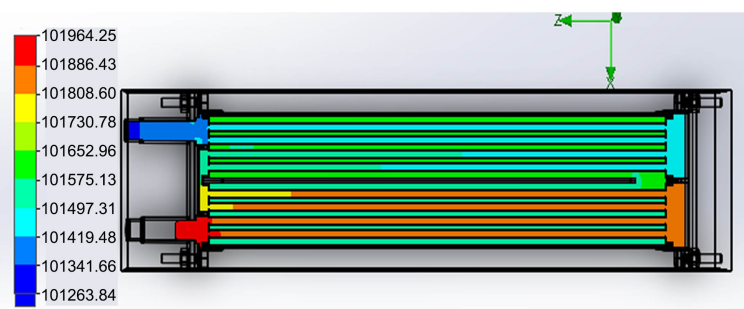
(a)



Velocity [m/s]

CS velocity cut plot: contours

(b)



Pressure [Pa]

CS pressure cut plot : contours

(c)

**Figure 5.** Contour cut plots for the cooling section heat exchanger (a) Temperature, (b) Velocity, (c) Pressure.

The tube-side fluid maintained a higher pressure within the tubes for the first and second pass compared to the third and fourth pass. There was a sharp drop in pressure as the fluid crossed from the second to the third pass (**Figure 5(c)**). The mean tube-side fluid pressure in the first, second, third, and fourth shell pass was 101.9 kPa, 101.8 kPa, 101.5 kPa, and 101.484 kPa, respectively. There was a significant reduction in the pressures ( $p < 0.05$ ) from the first to the fourth pass (**Table 5**).

**Table 5.** Variation of tube-side and shell-side temperature, velocity, and pressure along the fluid passes within the cooling section.

Pass	Tube-side (Mean $\pm$ SD)			Shell-side (Mean $\pm$ SD)		
	Temperature ( $^{\circ}$ C)	Velocity (m/s)	Pressure (kPa)	Temperature ( $^{\circ}$ C)	Velocity (m/s)	Pressure (kPa)
P1	54.23 $\pm$ 0.566 <sup>d</sup>	0.161 $\pm$ 0.0646 <sup>a</sup>	101.9 $\pm$ 0.0198 <sup>d</sup>	28.89 $\pm$ 1.336 <sup>a</sup>	0.104 $\pm$ 0.126 <sup>a</sup>	101.6 $\pm$ 0.0017 <sup>a</sup>
P2	52.06 $\pm$ 0.489 <sup>c</sup>	0.149 $\pm$ 0.0692 <sup>a</sup>	101.8 $\pm$ 0.0138 <sup>c</sup>	33.94 $\pm$ 3.492 <sup>b</sup>	0.033 $\pm$ 0.0161 <sup>a</sup>	101.6 $\pm$ 0.0061 <sup>b</sup>
P3	50.11 $\pm$ 0.589 <sup>b</sup>	0.154 $\pm$ 0.0621 <sup>a</sup>	101.5 $\pm$ 0.0274 <sup>b</sup>			
P4	48.25 $\pm$ 0.693 <sup>a</sup>	0.137 $\pm$ 0.0628 <sup>a</sup>	101.4 $\pm$ 0.0242 <sup>a</sup>			
p-value	<0.001	0.932	<0.001	0.008	0.203	< 0.001

P1, P2, P3, and P4 are the first, second, third, and fourth pass respectively. Means in the same column with different superscripts are significantly different ( $p < 0.05$ ).

#### 4.3.2. Shell-Side Fluid Temperature, Velocity, and Pressure in the Cooling Section

The shell-side fluid temperature was higher in the second than the first pass (**Figure 5(a)**). The mean shell-side fluid temperature was 28.89 $^{\circ}$ C and 33.94 $^{\circ}$ C for the first and second passes, respectively. Statistical analysis with ANOVA indicated a significant difference ( $p < 0.05$ ) in shell-side fluid temperatures between the shell-side passes (**Table 5**).

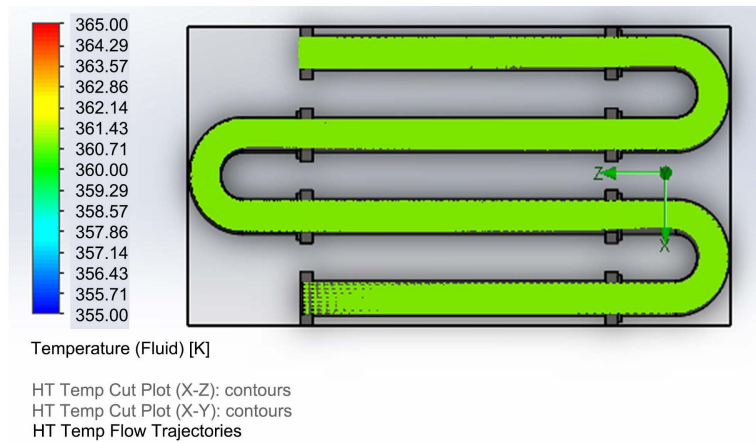
The shell-side fluid velocity was higher in the first pass compared to the second pass (**Figure 5(b)**). The mean shell-side velocity was maintained at 0.104 m/s and 0.033 m/s along the first and second, respectively. However, there was no significant difference ( $p < 0.05$ ) in the fluid velocities for the two passes (**Table 5**).

The shell-side fluid pressure was relatively high along the first pass but dropped significantly ( $p < 0.05$ ) during the second pass (**Figure 5(c)**, **Table 5**). The mean shell-side fluid pressure in the first and second pass was 101.59 kPa and 101.56 kPa, respectively.

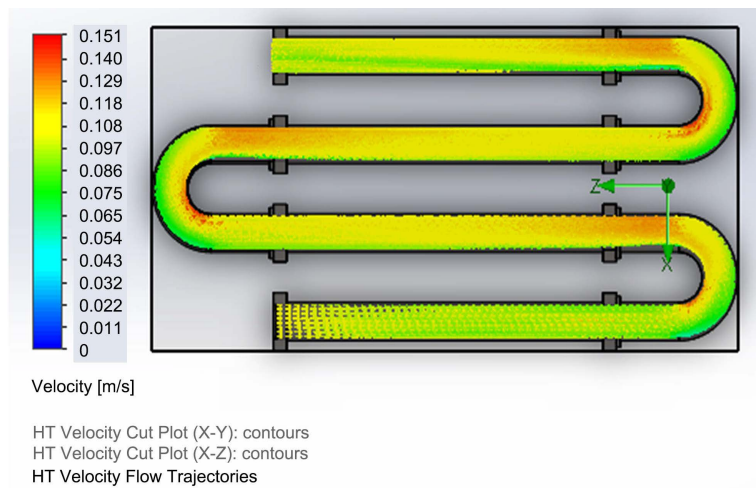
#### 4.4. Simulation of Temperature and Flow in Holding Tube

**Figure 6** shows the flow trajectories for the temperature, velocity, and pressure profiles for the holding tube. The temperature distribution in the holding tube is relatively uniform at 87.9 $^{\circ}$ C (**Figure 6(a)**). The velocity of flow ranges between 0.086 m/s and 0.129 m/s. The velocity is relatively uniform at about 0.108 m/s along the straight path in the holding tube. The velocity increases at the inner wall and reduces at the outer wall of the holding tube as the fluid approaches the U-bend. As the fluid leaves the bend, the velocity increases at the outer wall and reduces at the inner wall of the holding tube. This is the case at all bends along the holding tube (**Figure 6(b)**). Similar observations were made by López *et al.* [23]. The pressure decreases along the straight path of the holding tube (**Figure 6(c)**). The mean pressure was 101.338 kPa, 101.334 kPa, 101.329 kPa, and 101.325 kPa for the first, second, third, and fourth straight path respectively. There are high-pressure drops at the U-bends than along the straight path in the holding tubes (**Figure 6(c)**). The phenomenon of fluid flow and temperature distribution is synonymous with the results obtained by Dutta and Nandi [24].

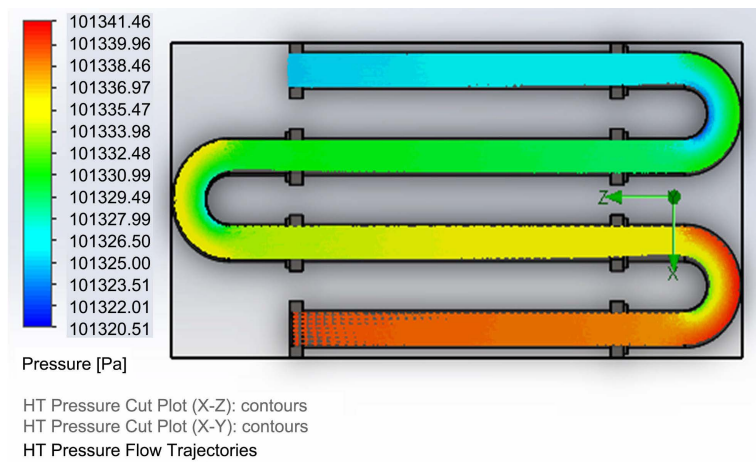
Zhang *et al.* [25] made similar observations in pressure drop with a 90-degree bend.



(a)



(b)



(c)

**Figure 6.** Flow trajectories for the holding tube (a) Temperature, (b) Velocity, (c) Pressure.

## 4.5. Discussion of Results

### 4.5.1. Simulation of Temperature and Flow in Heating, Regeneration, and Cooling Sections

The hot shell-side fluid flowing over the tubes in the heating and regeneration section allowed heat transfer from the shells to the tubes. On the other hand, the cold shell-side fluid runs over the tubes in the cooling section facilitating the cooling process. This could explain the increasing and decreasing trends in the tube-side and shell-side fluid temperatures respectively for the heating (**Table 3**) and regeneration section (**Table 4**). A similar argument explains increasing and decreasing trends in the shell-side and tube-side fluid temperatures respectively for the cooling section (**Table 5**). The significant variation ( $p < 0.05$ ) in temperature for both tube and shell-side fluids for all heat exchangers could be due to the overall heat transfer coefficient, large temperature difference, the length of the heat transfer surface, and residence time.

The larger cross-sectional area at the turning points compared to the tubes is responsible for low tube-side velocities at turning points. As the fluid enters the tube, there is an increase in volumetric flow rates thus increasing the flow velocity [26]. The small cross-section area for the tube compared to the shells is responsible for this higher mean tube-side than shell-side velocities for all heat exchangers (**Tables 3-5**). The larger the pipe diameter, the slower the flow velocity due to an increase in friction coefficient [27]. The lack of significant variation in tube-side and shell-side velocities along with different passes ( $p < 0.05$ ) within the heating, regeneration and cooling section is attributable to the uniform size of the tubes and shells.

The gradual pressure drop observed with the tube-side fluid along the tube's length for all heat exchangers is attributed to the frictional forces along the tube walls. The constrictions through which the fluid crossed from one shell to another increase the shell-side fluid velocity, explaining the significant pressure drop ( $p < 0.05$ ) on the shell-side fluid (**Tables 3-5**).

### 4.5.2. Simulation of Temperature and Flow in Holding Tubes

Along the straight path of the holding tube, the fluid particles move along the same direction of motion while the U-bend causes the fluid particles to change their direction of motion. This allows uniform mixing of the fluid thereby allowing proper distribution of heat within the fluid to contribute to the uniform temperature (**Figure 6(a)**). The uniform direction of motion is responsible for the relatively uniform velocity along the straight path of the holding tube (**Figure 6(b)**). At the curvature, the centrifugal force due to the change in direction of motion alters the position of maximum velocity from the center to some point between the center and the wall. The centrifugal force is inversely proportional to the radius of the circular path. The velocity is also directly proportional to the radius of the circular path. Therefore, the fluid far from the center of attraction runs at a relatively greater centrifugal force but lower velocity compared to the fluid near the center of attraction. This explains the higher velocities at the

inner wall of the pipe compared to the outer wall at the bends (**Figure 6(b)**). The energy losses resulting from fluid friction are responsible for the pressure loss along the straight path of the holding tube (**Figure 6(c)**). This drop could also be accelerated by the pressure drops at the U-bends [25]. The increase in velocity at the inner wall compared to the outer wall explains the lower pressure at the inner wall of the holding tube compared to the outer wall at the U-bends (**Figure 6(c)**). According to Bernoulli's principle, the higher the velocity of the fluid, the lower the pressure it exerts. The larger pressure drops at U-bends than in paths could be attributable to greater bend loss caused by centrifugal forces [28].

## 5. Conclusion

Computational fluid dynamics of the temperature and flow in the heat exchangers and the holding tubes of the continuous pasteurizer demonstrated that the current design has the potential to facilitate heat transfers and maintain the pre-determined holding temperature. The pasteurizer should be fitted with appropriate pumps to counter the negative effects to flow resulting from the pressure drops.

## Funding

This work was funded by the Eastern and Southern Africa Higher Education Centers of Excellence Project supported by World Bank MAPRONANO ACE, Makerere University (Project ID: P151847).

## Conflicts of Interest

The authors declare no conflicts of interest.

## References

- [1] Amit, S.K., Uddin, M.M., Rahman, R., Islam, S.M.R. and Khan, M.S. (2017) A Review on Mechanisms and Commercial Aspects of Food Preservation and Processing. *Agriculture & Food Security*, **6**, Article 51. <https://doi.org/10.1186/s40066-017-0130-8>
- [2] Watt, S. (2016) A Mini Review on Technique of Milk Pasteurization. *Journal of Pharmacognosy and Phytochemistry*, **5**, 99-101.
- [3] Peng, J., Tang, J., Barrett, D.M., Sablani S.S., Anderson, N. and Powers, J.R. (2017) Thermal Pasteurization of Ready-to-Eat Foods and Vegetables: Critical Factors for Process Design and Effects on Quality. *Critical Reviews in Food Science and Nutrition*, **57**, 2970-2895. <https://doi.org/10.1080/10408398.2015.1082126>
- [4] Indumathy, M., Sobana, S. and Panda, R.C. (2021) Modelling of Fouling in a Plate Heat Exchanger with High Temperature Pasteurisation Process. *Applied Thermal Engineering*, **189**, e116674. <https://doi.org/10.1016/j.applthermaleng.2021.116674>
- [5] Modi, A. and Prajapat, R. (2014) Pasteurization Process Energy Optimization for a Milk Dairy Plant by Energy Audit Approach. *International Journal of Scientific & Technology Research*, **3**, 181-188.
- [6] Escuder-Vieco, D., Espinosa-Martos, I., Rodriguez, J.M., Corzo, N., Montilla, A., Siegfried, P., *et al.* (2018) High-Temperature Short-Time Pasteurization System for Donor Milk in a Human Milk Bank Setting. *Frontiers in Microbiology*, **9**, Article

926. <https://doi.org/10.3389/fmicb.2018.00926>
- [7] Lewis, M.J. and Jun, S. (2012) Thermal Processing. In: Brennan, J.G. and Grandison, A.S., Eds., *Food Processing Handbook*, Wiley-VCH Verlag GmbH & Co. KGaA, Weinheim.
- [8] Ahumuza, A., Nabututa, E., Kigozi, J., Zziwa, A. and Sempira, E. (2017) Design, Construction and Performance Evaluation of an Automatic Batch Pasteurizer. *Journal of Advances in Food Science & Technology*, **4**, 145-154.
- [9] Ninshaba, P. (2015) Design and Construction of a Gas Heated Milk Pasteuriser. Busitema University, Busitema.
- [10] Jouhara, H., Khordehgh, N., Almahmoud, S., Delpech, B., Chauhan, A. and Tasou, S.A. (2018) Waste Heat Recovery Technologies and Applications. *Thermal Science and Engineering Progress*, **6**, 268-289. <https://doi.org/10.1016/j.tsep.2018.04.017>
- [11] Jonuskaite, A. (2017) Flow Simulation with SolidWorks. Arcada University of Applied Sciences, Helsinki.
- [12] Repko, T.W., Nix, A.C., Uysal, S.C. and Sisler, A.T. (2016) Flow Visualization of Multi-Hole Film-Cooling Flow under Varying Freestream Turbulence Levels. *Journal of Flow Control, Measurement & Visualization*, **4**, 13-29. <https://doi.org/10.4236/jfcmv.2016.41002>
- [13] Saha, S. and Majumdar, B. (2012) Flow Visualization and CFD Simulation on 65° Delta Wing at Subsonic Condition. *Procedia Engineering*, **38**, 3086-3096. <https://doi.org/10.1016/j.proeng.2012.06.359>
- [14] Bhuvanewari, E. and Anandharamkrishnan, C. (2014) Heat Transfer Analysis of Pasteurization of Bottled Beer in a Tunnel Pasteurizer Using Computational Fluid Dynamics. *Innovative Food Science and Emerging Technologies*, **23**, 156-163. <https://doi.org/10.1016/j.ifset.2014.03.004>
- [15] Bottani, E., Ferretti, G., Folezzani, M., Manfredi, M., Montanari, R. and Vignali, G. (2012) Modeling and Thermo-Fluid Dynamic Simulation of a Fresh Pasta Pasteurization Process. *International Journal of Food Engineering*, **9**, 327-339.
- [16] Bichkar, P., Dandgaval, O., Dalvi, P., Godase, R. and Dey, T. (2018) Study of Shell and Tube Heat Exchanger with the Effect of Types of Baffles. *Procedia Manufacturing*, **20**, 195-200. <https://doi.org/10.1016/j.promfg.2018.02.028>
- [17] Adumene, S., Nwaoha, T.C., Ombor, G.P. and Abam, J.T. (2016) Design and Off-Design Performance Evaluation of Heat Exchanger in an Offshore Process Configuration. *Open Access Library Journal*, **3**, e2748. <https://doi.org/10.4236/oalib.1102748>
- [18] Kanade, P. and Subramani, A. (2014) Hygienic Design Aspects of Pasteuriser to Assure Effective Pasteurisation of Milk. *Journal of Hygienic Engineering and Design*, **8**, 19-29.
- [19] Merritt, K. and Zhao, S. (2021) An Innovative Reflection Based on Critically Applying UX Design Principles. *Journal of Open Innovation: Technology, Market, and Complexity*, **7**, Article 129. <https://doi.org/10.3390/joitmc7020129>
- [20] Dunlap, S. (2017) Solidworks Fluid Flow Thermal Simulation to Enhance Solid State Drive Design. Master's Thesis, California State University, Sacramento.
- [21] Matsson, J.E. (2010) An Introduction to SolidWorks Flow Simulation. Schroff Development Corporation, Mission.
- [22] Widiatmo, J.S. and Hendrarsakti, J. (2018) Process Control of Milk Pasteurization using Geothermal Brine with Proportional Controller. *43rd Workshop on Geo-*

*thermal Reservoir Engineering*, Stanford, 12-14 February 2018, 1-10.

- [23] López, J., Ratkovich, N. and Pereyra, E. (2020) Analysis of Two-Phase Air-Water Annular Flow in U-Bends. *Heliyon*, **6**, e05818. <https://doi.org/10.1016/j.heliyon.2020.e05818>
- [24] Dutta, P. and Nandi, N. (2016) Effect of Bend Curvature on Velocity & Pressure Distribution from Straight to a 90° Pipe Bend-A Numerical Study. *REST Journal on Emerging Trends in Modelling and Manufacturing*, **2**, 103-108.
- [25] Zhang, J., Huang, H., Hu, K. and Zhang, P. (2020) Analysis of Elbow Effect on the High Pressure Gas Pipe. *Journal of Physics: Conference Series*, **1600**, e012087. <https://doi.org/10.1088/1742-6596/1600/1/012087>
- [26] Kanyiri, C.W., Kinyanjui, M. and Giterere, K. (2014) Analysis of Flow Parameters of a Newtonian Fluid through a Cylindrical Collapsible Tube. *SpringerPlus*, **3**, Article 566. <https://doi.org/10.1186/2193-1801-3-566>
- [27] Nur, A., Afrianita, R. and Ramli, R.D.T.F. (2019) Effect of Pipe Diameter Changes on the Properties of Fluid in Closed Channels Using Osborne Reynold Apparatus. *IOP Conference Series: Materials Science and Engineering*, **602**, e012058. <https://doi.org/10.1088/1757-899X/602/1/012058>
- [28] Ayegba, P.O., Edomwonyi-Out, L.C., Abubakar, A. and Yusuf, N. (2021) Flow Pattern and Pressure Drop for Oil-Water Flows in and Around 180° Bends. *SN Applied Sciences*, **3**, Article 10. <https://doi.org/10.1007/s42452-020-04031-z>